AUT Journal of Mechanical Engineering

AUT J. Mech. Eng., 6(3) (2022) 467-488
DOI: 10.22060/ajme.2022.20383.5997

A Parametric Investigation of Melting Process within a Porous Medium under Local Thermal Non-Equilibrium Condition Using Lattice Boltzmann Method

M. Taghilou* , S. A. Safavi

Department of Engineering, University of Zanjan, Zanjan, Iran

ABSTRACT: The use of a porous medium with a high conductivity improves the rate of heat transfer in latent energy storage systems. This paper investigates the melting of the phase change material inside a porous medium under the local thermal non-equilibrium condition with the lattice Boltzmann method. Results examine the effect of Rayleigh number, porosity ratio, pore size, and Sparrow number on the liquid fraction and position of the melting front. Results show that by increasing the pore diameter, the interface of the two phases tends to bend but the liquid fraction decreases. Also, it is found that the difference between the liquid fraction in the presence and absence of natural convection for $Ra<10^6$, is less than 5%. Nonetheless, by increasing the Rayleigh number to 10^8, this difference at Fo=0.003 is more than 14% and at Fo=0.006 will reach more than 31%. Furthermore, in $Ra=10^8$ and for small Sparrow numbers, this difference is small and intensifies with increasing the Sparrow number. Also, by reducing the Darcy number, natural convection is weakened and it can be ignored for $Da<10^{-4}$. It is shown that in small Darcy numbers $Da=10^{-4}$, the deviation from the pure conduction is always increased by Sparrow number, and for larger Darcy numbers $Da=10^{-2}$, this deviation has a maximum value of 53% at Fo=0.003 and 84% at Fo=0.006.

Review History:

Received: Aug. 07, 2021
Revised: May, 05, 2022
Accepted: Jun. 27, 2022
Available Online: Jul. 01, 2022

Keywords:

Porous medium, Local thermal non-equilibrium condition
Melting process
Natural convection
Lattice Boltzmann method

1- Introduction

Energy cost, its scarcity, as well as environmental problems have become a recent concern for researchers. The storage of thermal energy in both sensible and latent forms can be proposed as a solution for the management of energy consumption [1, 2]. Phase Change Materials (PCMs) with a high capacity of energy storage and nearly constant temperature of melting and solidification can be referred to as Latent Heat Thermal Storage (LHTS) systems. Nonetheless, PCMs suffer from the low thermal conductivity that increases the phase change time as well as the temperature gradient inside the energy storage reservoir in large-scale applications. There are various strategies to eliminate this weakness, including metal fins [3, 4], adding nanoparticles into the PCM [5, 6], and placing a porous medium with a high thermal conductivity inside the reservoir [7, 8].

Tao et al. [9] examined the problem of heat transfer with phase change in the composites including paraffin and metal foams using the Lattice Boltzmann Method (LBM). They defined a new parameter, which represents the number of Pores Per Inch (PPI) of the composite material. The results showed that increasing the PPI increases the conduction heat transfer and decreases the natural convection in the liquid phase of the PCM. Jourabian et al. [10] presented a numerical study to simulate the ice melting inside a rectangular cavity with two vertical cylinders using a metallic porous matrix. They used enthalpy-based LBM with a double distribution function with the local thermal equilibrium between porous structure and ice. It is shown that inserting the porous medium into the PCM enhances the heat conduction and weakens the natural convection. Gao et al. [11] presented a modified lattice Boltzmann model to simulate the melting of the PCM inside a porous medium with conducting fins. Results showed that the long fins with low heat capacity increase the rate of melting. Gao and Chen [12] investigated the problem of melting with natural convection in a rectangular cavity containing a porous medium using LBM. They studied the effect of Darcy number, Rayleigh number, and porosity on the melting process and also continued to study the problem of solidification with the same model. Results showed that with increasing the Rayleigh and Darcy numbers and increasing the porosity, the natural convection in the liquid phase is strengthened, which bends the melting front.

The use of a porous medium with a high thermal conductivity increases the rate of melting and freezing in the PCM. Nevertheless, the difference in thermal conductivity between the porous medium and the PCM can expire the Local Thermal Equilibrium (LTE) condition between the PCM and the porous medium [13, 14]. Under the Local Thermal Non-Equilibrium (LTNE) condition, two energy equations should be solved simultaneously to obtain the temperature distribution of the PCM and the porous medium. Gao et al. [15] used the LBM to investigate the natural convection in a

*Corresponding author's email: taghilou@znu.ac.ir

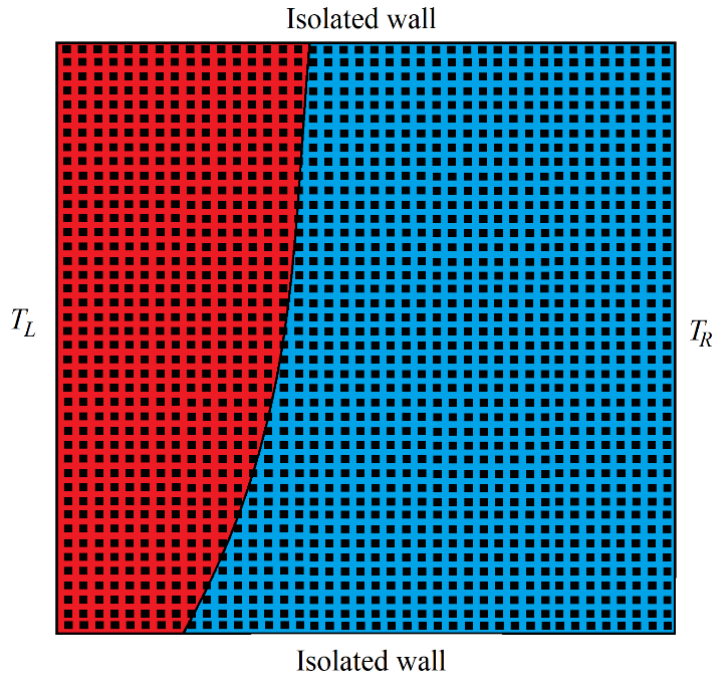

Fig. 1. Schematic of melting problem inside a porous medium.

porous medium under the LTNE condition. They used three distribution functions: one is for calculating the velocity field and the other two distribution functions compute the temperature field of the operating fluid and the porous medium. It is shown that if the thermal conductivity of the porous medium to the thermal conductivity of the working fluid is large and the Nusselt number is small, the LTE assumption is not reliable. In another study, Gao et al. [13] proposed an improved LBM for the problem of solid-liquid phase change in a porous medium under local thermal non-equilibrium conditions. They used the total enthalpy method and defined a free parameter to reduce the induced numerical diffusion due to phase change. Wang et al. [16] studied unsteady heat transfer in the porous medium focusing on the necessary condition to apply the LTNE condition. They used the Sparrow number as equilibrium conduction to the convection thermal resistances. They concluded that for the high Sparrow numbers LTE condition is provided. Esapour et al. [17] investigated the melting and solidification of the PCM embedded in metallic porous foam inside a multi-tube heat exchanger. They assumed the LTNE condition and examined the effects of inner tubes and porous medium on the melting and solidification of the PCM. They concluded that the use of porous medium is more efficient in the solidification process rather than the melting. Liu et al. [18] proposed a new LBM for the convective heat transfer within a porous medium under the LTNE condition. The advantage of this model is its simplicity compared to the previous models.

The authors found that there is no parametric study that shows the simultaneous effects of natural convection and local thermal non-equilibrium condition within the liquid phase on the melting process of the PCMs. Therefore, the process of melting of the PCM in a porous medium is simulated numerically considering the local thermal non-equilibrium condition with the LBM and the effects of parameters such as Rayleigh number, porosity ratio, pore size, and Sparrow number on the liquid fraction and position of the melting front are investigated. Also, conditions in which the role of natural convection in the melting process is low and negligible are introduced.

2- Problem Definition

Consider a two-dimensional square container which is completely filled with phase change material and a uniform porous medium. According to Fig. 1, the upper and lower boundaries are thermally insulated and the right and left boundaries are subject to a constant temperature. The initial and right wall temperatures are equal to the melting temperature in such a way that the initial state of the phase change material is solid. At the beginning of the process, the temperature of the left wall is increased slightly above the melting temperature to start the melting process.

The temperature of the boundaries as well as the melting temperature in the dimensionless form and domain dimension are stated in section 5-1. For the sake of simplicity and to avoid unnecessary computations, the numerical model benefits from the following assumptions:

1.The effects of flow and fluid compressibility are neglected. To take into account the effects of natural convection, the Boussinesq approximation is used.

2.The PCM is assumed to be ideal. The ideal of PCM means its behavior is isotropic and free of impurities.

3.The thermophysical properties of each phase are considered different from another phase but are independent of temperature.

3- Mathematical Modeling

3- 1- Macroscopic equations

Due to the presence of the local thermal non-equilibrium condition, it is necessary to solve the energy equations for the PCM and porous medium, separately. Macroscopic energy equations for the PCM and porous medium are expressed as follows [13]:

$$\varepsilon\frac{\partial\left[\left(\rho c_p\right)_f T_f\right]}{\partial t}+\nabla.\left[\left(\rho c_p\right)_{fl}\mathbf{u}T_f\right]= k_{e,f}\nabla^2T_f+h_v\left(T_s-T_f\right)-\varepsilon\rho_{fl}L_a\frac{\partial f_l}{\partial t} \tag{1}$$

$$\left(1-\varepsilon\right)\frac{\partial\left[\left(\rho c_p\right)_s T_s\right]}{\partial t}=k_{e,s}\nabla^2T_s+h_v\left(T_f-T_s\right) \tag{2}$$

where subscripts f, s, and fl express the PCM, porous medium, and liquid phase of the PCM, respectively. In these equations; u, T, c_p, L_a, and f_l represent the fluid velocity, temperature, specific heat capacity, latent heat, and liquid fraction of the PCM. Also, ε is the porosity, $k_{e,f}$, and $k_{e,s}$ refer to the effective conductivity of the PCM and porous medium and h_v stands for the volumetric convective heat transfer coefficient due to the local thermal non-equilibrium condition between the PCM and porous medium. By defining the total enthalpy for the PCM $En_f=\left(\rho c_p\right)_f T_f+\rho L_a f_l$ and the porous medium $En_s=\left(\rho c_p\right)_s T_s$, Eqs. (1) and (2) will be rewritten as:

$$\varepsilon\frac{\partial En_f}{\partial t}+\nabla.\left[\left(\rho c_p\right)_{fl}\mathbf{u}T_f\right]=k_{e,f}\nabla^2T_f+h_v\left(T_s-T_f\right) \tag{3}$$

$$\left(1-\varepsilon\right)\frac{\partial\left[En_s\right]}{\partial t}=k_{e,s}\nabla^2T_s+h_v\left(T_f-T_s\right) \tag{4}$$

Also, the macroscopic equations for the mass and momentum conservations for the porous medium are expressed as follows [13]:

$$\nabla.\mathbf{u}=0 \tag{5}$$

$$\frac{\partial\mathbf{u}}{\partial t}+\left(\mathbf{u}.\nabla\right)\left(\frac{\mathbf{u}}{\varepsilon}\right)=-\frac{1}{\rho_{fl}}\nabla\left(\varepsilon p\right)+\upsilon_e\nabla^2\mathbf{u}+\mathbf{F} \tag{6}$$

In the above equations, p and υ_e are pressure and effective kinematic viscosity, respectively. F represents the total volumetric forces resulted from the porous medium and other body forces and is expressed by [13]:

$$\mathbf{F}=-\frac{\varepsilon\upsilon_{fl}}{K}\mathbf{u}-\frac{\varepsilon F_\varepsilon}{\sqrt{K}}\left|\mathbf{u}\right|\mathbf{u}+\varepsilon\mathbf{g}\beta\left(T_f-T_{ref}\right) \tag{7}$$

In Eq. (7), υ_{fl}, F_ε, K, β, T_{ref}, and g are the kinematic viscosity of the fluid, the Forchheimer coefficient, permeability, thermal expansion coefficient, the reference temperature, and the gravitational acceleration, respectively. The dimensionless parameters that control the fluid flow along with heat transfer and the phase change phenomenon are Prandtl number Pr, Rayleigh number Ra, Darcy number Da, Stefan number Ste, Nusselt number Nu_d and porosity ratio ε. These parameters along with other important non-dimensional parameters are defined by:

$$\begin{aligned} &Pr=\frac{\upsilon_{fl}}{\alpha_{fl}},\quad Ra=\frac{g\beta\left(T_L-T_R\right)L^3}{\upsilon_{fl}\alpha_{fl}},\quad Da=\frac{K}{L^2},\\ &Ste=\frac{c_{p,fl}\left(T_L-T_R\right)}{L_a},\quad Nu_d=\frac{h_v d_p^2}{k_{fl}}\\ &\varepsilon=\frac{V_p}{V},\quad T^*=\frac{T-T_R}{T_L-T_R},\quad Fo=\frac{\alpha_f t}{L^2},\\ &\eta=\frac{\left(\rho c_p\right)_s}{\left(\rho c_p\right)_{fl}},\quad \delta=\frac{d_p}{L},\quad J=\frac{\upsilon_e}{\upsilon_{fl}} \end{aligned} \tag{8}$$

In the above definitions, L, d_p, V_p, V, T^*, and Fo indicate the characteristic length of the enclosure, the pore diameter, the volume of empty space, the total volume of the space, the dimensionless temperature, and the dimensionless time.

3- 2- Local thermal non-equilibrium condition

The dimensionless number that controls the thermal non-equilibrium condition is the Sparrow number. Here, the Sparrow number, Sp, and the equivalent thermal conductivity of the medium k_e are defined by:

$$Sp=\frac{h_v L^3}{k_e d_p} \tag{9}$$

$$k_e=\varepsilon k_{fl}+\left(1-\varepsilon\right)k_s \tag{10}$$

By defining the Nusselt number based on the hydraulic radius of the pores, Eq. (9) becomes Eq. (11).

$$Sp=Nu_d\left(\frac{k_{fl}}{k_e}\right)\left(\frac{L}{d_p}\right)^3 \tag{11}$$

4- Lattice Boltzmann Modeling

4- 1- Fluid flow inside a porous medium

The distribution function for the velocity field f_i is given by [13]:

$$f_i\left(\mathbf{r}+\mathbf{e}_i\delta t,t+\delta t\right)-f_i\left(\mathbf{r},t\right)= -\frac{1}{\tau}\left[f_i\left(\mathbf{r},t\right)-f_i^{eq}\left(\mathbf{r},t\right)\right]+\delta t F_i \tag{12}$$

where r and e_i are lattice positions and discretized lattice velocities and Δt is the time step indicator. Also, f_i^{eq} is the equilibrium distribution function for the velocity field, which is defined by [13]:

$$f_i^{eq}=w_i\rho[1+\frac{\mathbf{e_i}.\mathbf{u}}{c_s^{\,2}}+\frac{(\mathbf{e_i}.\mathbf{u})^2}{2\varepsilon c_s^{\,4}}-\frac{\mathbf{u}^2}{2\varepsilon c_s^{\,2}}] \tag{13}$$

where w_i states weight coefficient and are given by:

$$w_i=\begin{cases}4/9, & i=0\\ 1/9, & i=1-4\\ 1/36, & i=5-8\end{cases} \tag{14}$$

and $c_s=1/\sqrt{3}$ represent the sound velocity.

The discrete body force F_i can be expressed by [13]:

$$F_i=w_i(1-\frac{1}{2\tau})\rho\left[\frac{\mathbf{e_i}.\mathbf{F}}{c_s^2}+\frac{\mathbf{uF}:\mathbf{e_i}\mathbf{e_i}}{\varepsilon c_s^4}-\frac{\mathbf{u}.\mathbf{F}}{\varepsilon c_s^2}\right] \tag{15}$$

The density ρ and fluid velocity u can be obtained as follows [19]:

$$\rho(\mathbf{r},t)=\sum_{i=0}^{8}f_i(\mathbf{r},t) \tag{16}$$

$$\mathbf{u}=\frac{\mathbf{v}}{d_0+\sqrt{d_0^{\,2}+d_1|\mathbf{v}|}} \tag{17}$$

where

$$\mathbf{v}=\sum_{i=0}^{8}\frac{\mathbf{e}_i f_i}{\rho}+\frac{\Delta t}{2}\varepsilon\left[\mathbf{g}\beta(T_f-T_{ref}\right] \tag{18}$$

In Eq. (17), d_0 and d_1 are known using $d_0=\frac{1}{2}\left(1+\frac{\varepsilon\Delta t\upsilon_{fl}}{2K}\right)$ and $d_1=\frac{\varepsilon\Delta t F_\varepsilon}{2\sqrt{K}}$, respectively. The dimensionless relaxation time is expressed according to Eq. (19):

$$\tau=\frac{\upsilon_e}{c_s^2\delta t}+0.5 \tag{19}$$

Note that the velocity field inside the solid phase is considered zero.

4- 2- Temperature field for PCM and solid matrix

The distribution function for the temperature field of the PCM, $g_{i,f}$, and the solid matrix, $g_{i,s}$ are expressed according to Eqs. (20) and (21), respectively [13]:

$$g_{i,f}\left(\mathbf{r}+\mathbf{e}_i\delta t,t+\delta t\right)-g_{i,f}\left(\mathbf{r},t\right)= -\frac{1}{\tau_{t,f}}\left[g_{i,f}\left(\mathbf{r},t\right)-g_{i,f}^{eq}\left(\mathbf{r},t\right)\right]+\left(\delta t+\frac{\delta t^2}{2}\partial t\right)Sr_{i,f}+\delta t Su_{i,f} \tag{20}$$

$$g_{i,s}\left(\mathbf{r}+\mathbf{e}_i\delta t,t+\delta t\right)-g_{i,s}\left(\mathbf{r},t\right)= -\frac{1}{\tau_{t,s}}\left[g_{i,s}\left(\mathbf{r},t\right)-g_{i,s}^{eq}\left(\mathbf{r},t\right)\right]+\left(\delta t+\frac{\delta t^2}{2}\partial t\right)Sr_{i,s} \tag{21}$$

Relaxation times for the temperature of the PCM $\tau_{t,f}$, and solid matrix $\tau_{t,s}$ are defined by:

$$\tau_{t,f}=\frac{\alpha_f}{c_s^2}+0.5,\quad \tau_{t,s}=\frac{\alpha_s}{c_s^2}+0.5 \tag{22}$$

Also, the equilibrium distribution functions for the temperature of PCM and solid matrix are expressed as [13]:

$$g_{i,f}^{eq}=\begin{cases}\varepsilon En_f-\gamma_f T_f+w_i\gamma_f T_f, & i=0\\ w_i T_f\left(\gamma_f+\left(\rho c_p\right)_{fl}\frac{e_i.\vec{u}}{c_s^2}\right), & i\neq 0\end{cases} \tag{23}$$

$$g_{i,s}^{eq}=\begin{cases}(1-\varepsilon)En_s-\gamma_s T_s+w_i\gamma_s T_s, & i=0\\ w_i\gamma_s T_s, & i\neq 0\end{cases} \quad (24)$$

where γ_f and γ_s are two free parameters for the liquid and solid phases, respectively. In Eqs. (20) and (21), Sr and Su are two source terms and are expressed by the following relations [13]:

$$Sr_{i,f}=w_i h_v\left(T_s-T_f\right) \quad (25)$$

$$Sr_{i,s}=w_i h_v\left(T_f-T_s\right) \quad (26)$$

$$Su_{i,f}=w_i\left(1-\frac{1}{2\tau_{t,f}}\right)\frac{\mathbf{e}_i}{c_s^2}\cdot\frac{\partial\left[\left(\rho c_p\right)_{fl}T_f\mathbf{u}\right]}{\partial t} \quad (27)$$

Finally, the total enthalpy of the PCM En_f and solid matrix En_s can be calculated with the following equations [13]:

$$En_f=\sum_{i=0}^{8}\frac{g_{i,f}}{\varepsilon} \quad (28)$$

$$En_s=\sum_{i=0}^{8}\frac{g_{i,s}}{1-\varepsilon} \quad (29)$$

Then, by having the enthalpy, the temperature and the liquid fraction of the PCM f_l liquid can be calculated [13]:

$$T_f=\begin{cases}T_{begin}-\dfrac{En_{begin}-En_f}{\left(\rho c_p\right)_{fs}}, & En_f\le En_{begin}\\ \dfrac{En_{end}-En_f}{En_{end}-En_{begin}}T_{begin}+\dfrac{En_f-En_{begin}}{En_{end}-En_{begin}}T_{end}, & En_{begin}<En_f<En_{end}\\ T_{end}+\dfrac{En_f-En_{end}}{\left(\rho c_p\right)_{fl}}, & En_f\ge En_{end}\end{cases} \quad (30)$$

$$f_l=\begin{cases}0, & En_f\le En_{begin}\\ \dfrac{En_f-En_{begin}}{En_{end}-En_{begin}}, & En_{begin}<En_f<En_{end}\\ 1, & En_f\ge En_{end}\end{cases} \quad (31)$$

In the above equations, subscripts of begin and end refer to the beginning and end of the phase change. Also, $En_{begin}=\left(\rho c_p\right)_{fs}T_{begin}$ is the total enthalpy at the beginning of the phase change and $En_{end}=\left(\rho c_p\right)_{fl}T_{end}+\rho_{fl}L_a$ is the total enthalpy at the end of the phase change process.

Note that the equations for the velocity and energy distribution functions are written in the FORTRAN programming language.

4- 3- Boundary condition

Any distribution function N_i at each point can be considered as a sum of equilibrium N_i^{eq} and non-equilibrium N_i^{neq} parts such as [20]:

$$N_i=N_i^{eq}+N_i^{neq} \quad (32)$$

Since the distribution functions coming from the outside of the domain are not known after streaming, the non-equilibrium part cannot be obtained at the collision step at the boundary points. To yield the distribution function at the boundary point, $N_{i,b}$ the equilibrium part $N_{i,b}^{eq}$ is computed owning to the macroscopic parameter at the boundary and corresponding equilibrium equation. But the non-equilibrium part $N_{i,b}^{neq}$ could be estimated by the first order extrapolation with neighbor points, $N_{i,n}^{neq}$. Knowing that $N_{i,n}^{neq}=N_{i,n}-N_{i,n}^{eq}$ Eq. (32) at the boundary points is written as:

$$N_{i,b}=N_{i,b}^{eq}+\left(N_{i,n}-N_{i,n}^{eq}\right) \quad (33)$$

Hence, the collision term for the boundary points can be obtained as follows:

$$N_{i,b}^{*}=N_{i,b}^{eq}+\left(1-\frac{1}{\tau_N}\right)\left(N_{i,n}-N_{i,n}^{eq}\right) \quad (34)$$

In Eq. (34), $N_{i,b}^{*}$ is the post-collision distribution function, and τ_N is the relaxation time related to the N.

Knowing the macroscopic quantities at the boundaries makes it possible to use Eq. (34) and calculate the equilibrium distribution function at the boundaries. According to Fig. 1 and referring to Table 1, the distribution function at the boundaries can be calculated.

Note that in the insulation boundary condition, the use of first-order discretization determines the value of temperature at the boundary, and then similar to the constant temperature boundary condition, the distribution function is obtained.

Table 1. Boundary conditions applied in the present problem.

	Left wall	Right wall	Upper wall	Bottom wall
Boundary condition	$T=T_L$	$T=T_R$	$\partial T/\partial n=0$	$\partial T/\partial n=0$

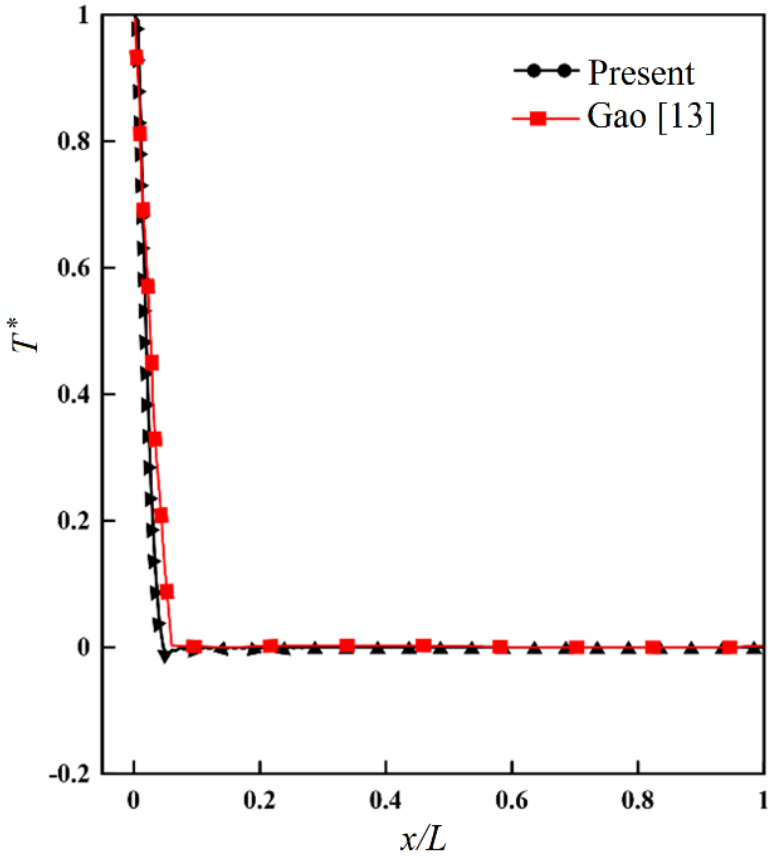

Fig. 2. Temperature of the PCM on the line passing through the middle of the enclosure (y/L=0.5) at Fo=0.002 for the case of LTE.

5- Results and Discussion

Here, the effect of natural convection on the melting rate of the PCM in a porous medium with a high difference in the thermal conductivities of PCM and solid matrix are investigated. The high difference in the thermal conductivities causes a thermal non-equilibrium condition at the interface of the PCM and the solid matrix. Before examining the effects of natural convection on the temperature field and liquid fraction, it is necessary to ensure the correct operation of the written code.

5- 1- Model verification

Numerical results of Gao et al. [13] have been used to validate the present work. For this purpose, first, the melting problem in a porous medium with local thermal equilibrium condition is solved and then the melting process with local thermal non-equilibrium is considered. In this regard, a square domain with upper and lower adiabatic walls and constant temperature on the left and right walls is intended. At the beginning of the process, the PCM and solid matrix are both at the initial temperature $T_{in}^{*}=0$, and the temperature of the left wall T_L^{*} suddenly rises to 1, and the temperature of the right wall T_R^{*} is set to 0. The dimensions of the computational domain have been selected as 150×150. The detailed numerical values for all parameters are given in Table 2.[13].

The conditions corresponding to the numerical values in Table 2 are considered as base conditions and are used as reference values in the following sections. In the first step of the validation, the melting temperature is the same as the initial temperature ($T_{melt}^{*}=T_{in}^{*}=0$) and due to the local thermal equilibrium condition, the Nusselt number is equal to zero, Nu_d=0. Fig. 2 shows the temperature of the PCM on the

Table. 2. The detailed numerical values for all parameters used in the base condition [13].

ε	δ	Pr	Da	Ra	Ste	Sp	F_ε	η	Nu_d	T^*_{melt}	$\tau_{t,f}$
0.8	0.0135	50	10^{-4}	10^8	1	12000	0.068	1	5.9	0.3	0.501

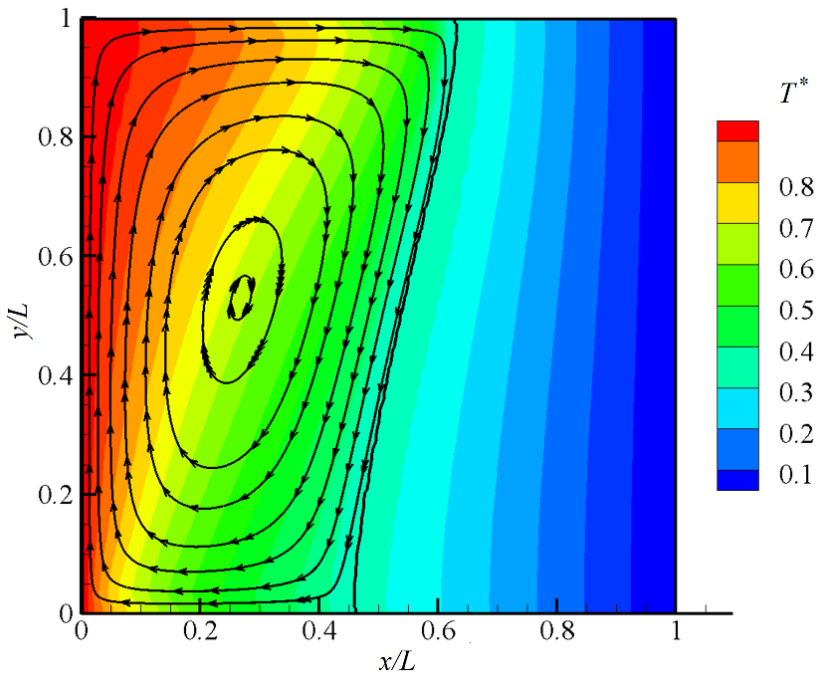

Fig. 3. Temperature contour for the PCM at Fo=0.002 specified by the color spectrum in 9 levels along with streamlines in the liquid phase (base condition).

line passing through the middle of the enclosure (y/L=0.5) at Fo=0.002. It is seen that for the case of Nu_d=0, a good agreement appears between the present simulation and the results of the test case [13]. Next, the validation is performed for the condition where the local thermal non-equilibrium condition exists. All numerical parameters are the same as in Table 2.

Fig. 3 shows the temperature contours for the PCM by the color spectrum in 9 levels along with the position of the melting front and the streamlines within the liquid phase at Fo=0.002. According to this figure, it is observed that the presence of natural convection within the liquid phase causes two-dimensional heat transfer and bending of the melting front.

Similarly, Fig. 4 shows the temperature contours for the porous medium by solid lines at 9 levels with streamlines at Fo=0.002. In order to compare the temperature fields of the PCM and porous medium, the PCM temperature is also shown by the color spectrum in 9 levels.

According to the figure, it can be seen that the existence of the local thermal non-equilibrium condition has caused a difference between the temperatures of these two media so that this temperature difference is greater in the liquid phase and at the top and bottom of the enclosure. Note that the flow velocity in these two zones is higher and therefore the difference in temperature between the PCM and the porous medium can be attributed to natural convection. Fig. 5 represents a comparison of the position of the melting front between the present simulation and the previous results [13] at Fo=0.0004, Fo=0.002, and Fo=0.006. Comparing the position of the melting front with the results of Gao et al. [13] shows a slight difference in predicting the melting position. This discrepancy can occur for two reasons. The first reason is the existence of a time derivative in Eqs. (20) and (21). In the present paper, the forward second-order discretization is used (the first stage is forward first-order), while in Ref. [13] the derivation method is not mentioned. The second reason can also be related to the satisfaction of incompressibility conditions, which is also not considered by Gao et al. The local Mach number at each point of the flow must be small enough to ensure the incompressibility of the flow. In the case of natural convection, the criterion used to ensure the incompressibility of the flow is introduced as $g\beta\Delta TH < 0.1$ [21].

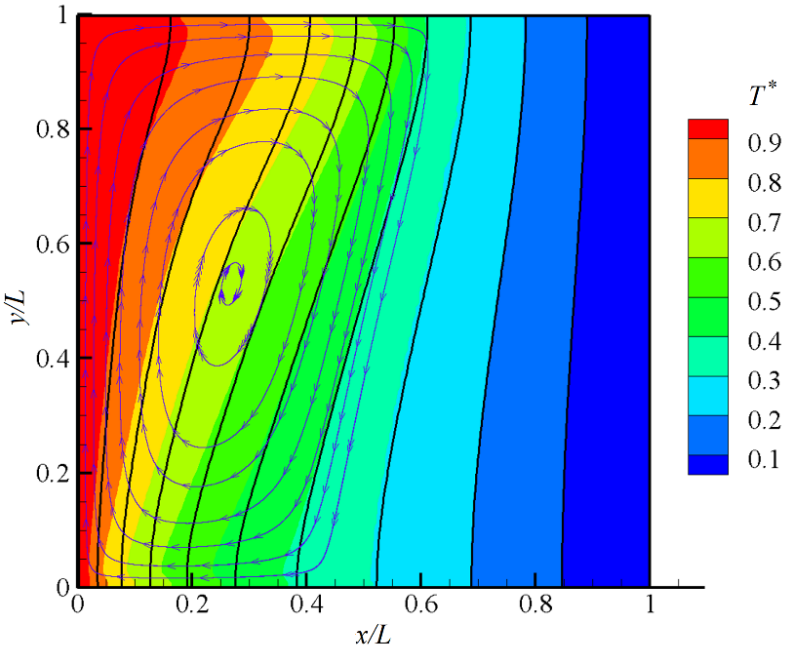

Fig. 4. Temperature contour for the porous medium specified by solid lines in 9 levels along with streamlines in the liquid phase. To compare the temperature of PCM and porous medium, the temperature of the PCM is given as a color spectrum.

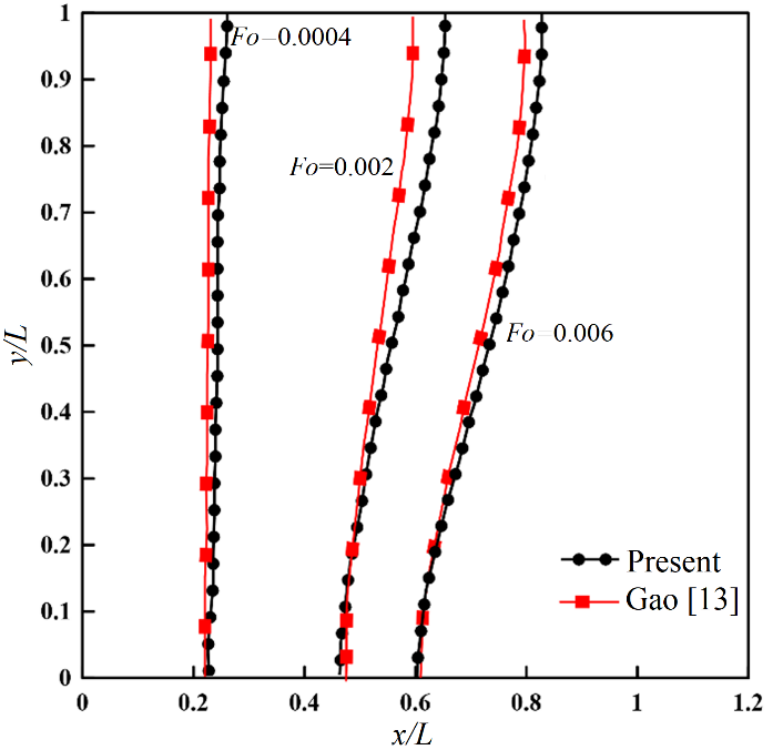

Fig. 5. Position of the melting front at Fo=0.0004, Fo=0.002, and Fo=0.006 for the case of LTNE.

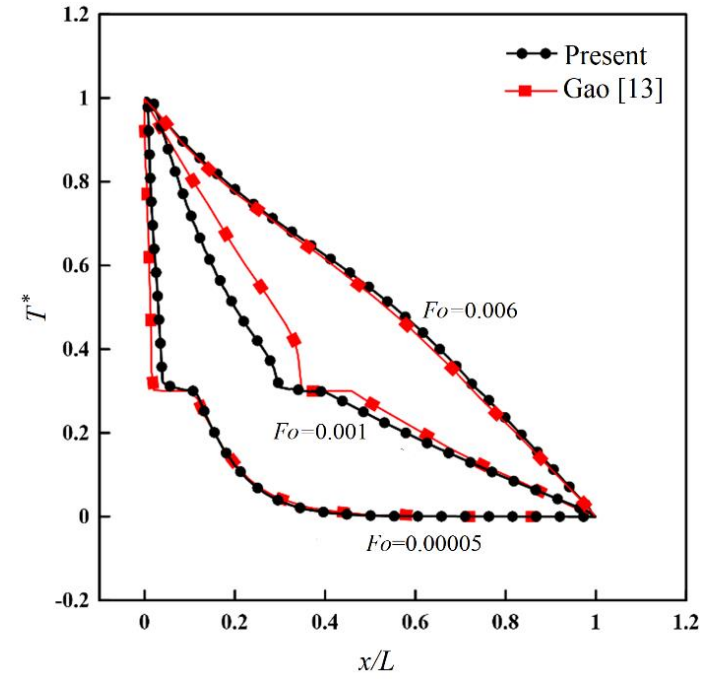

a

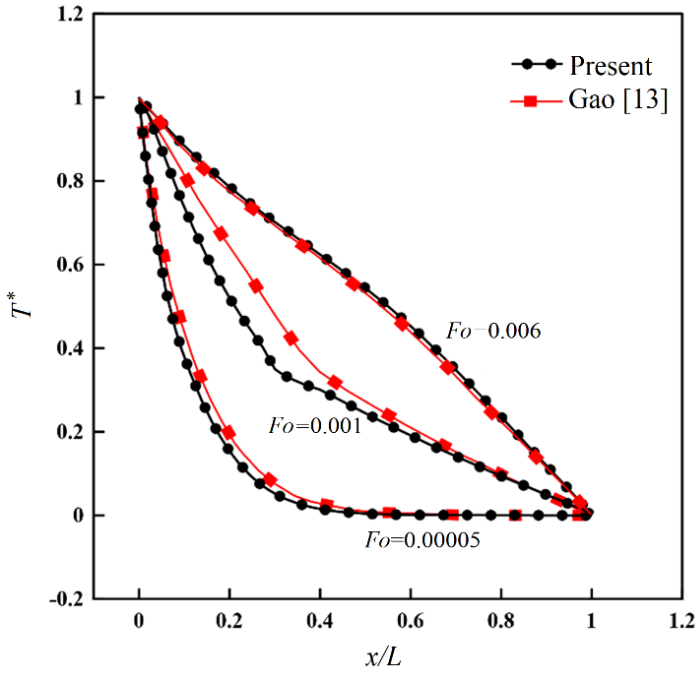

b

Fig. 6. Validation of numerical modeling with those of Gao et al. [13] for the case of LTNE, a) temperature of the PCM and b) temperature of the solid matrix.

In order to compare the temperature distribution obtained in the present work with Gao et al. [13], the temperature values of PCM and the porous medium are plotted on a horizontal line passing through the middle of the domain at Fo=0.00005, Fo=0.001, and Fo=0.006 in Figs, 6a, and 6b, respectively. It is seen that the difference between the temperature distribution of PCM and the porous medium of the two works is small except at Fo=0.001, which is not clear to the authors.

In the following, the effect of changes in the Rayleigh number, Nusselt number, porosity ratio, the ratio of pore diameter to the characteristic length of the enclosure, and the Sparrow numbers on the liquid fraction and melting front is investigated. Finally, the conditions under which the natural convection during the melting process can be ignored are expressed.

Table. 3. The detailed numerical values for all parameters used in case 1 (Effect of Rayleigh number)

ε	δ	Pr	Da	Ste	Sp	F_ε	η	Nu_d	T^*_{melt}	$\tau_{t,f}$
0.8	0.0135	50	10^{-2}	1	12000	0.068	1	5.9	0.3	0.501

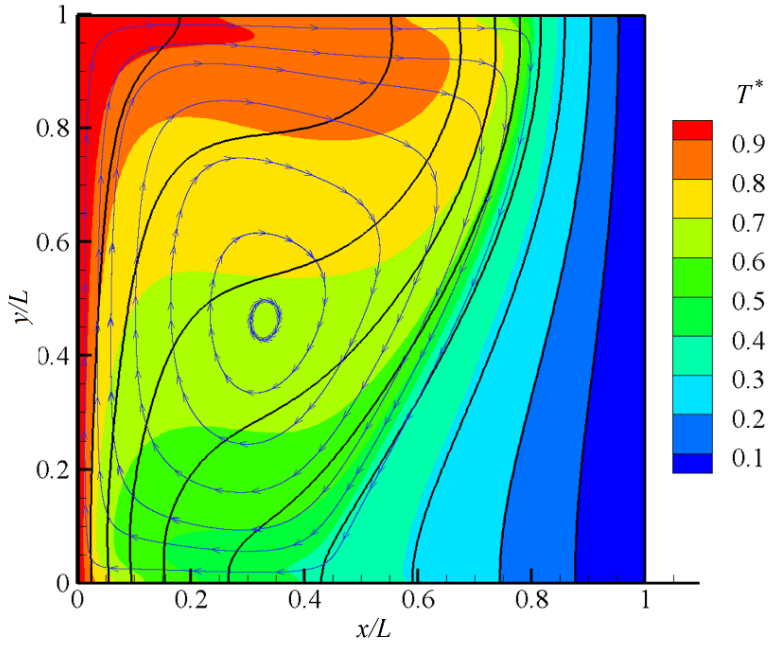

Fig. 7. Temperature contour for the PCM and porous medium at Fo=0.002 specified by the color spectrum and solid lines, respectively, in 9 levels along with streamlines in the liquid phase (Da=10-2).

5- 2- Effect of Rayleigh number

To evaluate the effect of the Rayleigh number, four values of Ra=0, Ra=10^6, Ra=10^7, and Ra=10^8 have been used, and the rest of the parameters are according to Table 3. This case is called case 1.

Fig. 7 shows the temperature contours for the PCM and the porous medium at Fo=0.002 by the color spectrum and solid lines at 9 levels, respectively. A comparison of this figure with Fig. 4 shows that with increasing the Darcy number and increasing the permeability of the porous medium, the amount of liquid fraction has increased. It is also observed that the temperature difference between the PCM and the porous medium increases, which is due to the strengthening of the velocity field due to the increase in the permeability of the porous medium.

Fig. 8 shows the effect of the Rayleigh number on the liquid fraction. As shown in this figure, as the Rayleigh number increases, the liquid fraction increases, which is because as the Rayleigh number increases, the natural convection enhances, and speeds up the melting process. It is also seen that for Ra=0 and Ra=10^6 the values of the liquid fraction are similar, which means that up to Rayleigh 10^6 contribution of the natural convection is weak. Fig. 9 shows the position of the melting front for different Rayleigh numbers at Fo=0.002. According to Fig. 9, it is quite clear that with the increase of the Rayleigh number, the curvature of the melting front increases, and natural convection plays a more important role in the melting process.

It is also seen that up to Ra=10^6, the melting front has a very small curvature, so that a similar amount of deviation in the upper half of the enclosure, occurs approximately at the bottom of the enclosure. For this reason, the change of the liquid fraction in the presence of natural convection in the range of Ra=0 to Ra=10^6 does not change significantly compared to the pure conduction state. Fig. 10 shows the temperature of the middle node of the cavity, T_p^* with time. This diagram consists of three parts: pure conductive heat transfer (temperature growth at the beginning of the diagram), mushy zone (nearly constant temperature of the diagram), and heat transfer with natural convection (sudden increase in temperature after the mushy zone). As shown in Fig. 10, with increasing the Rayleigh number, the mushy zone becomes smaller and the temperature of the node in the middle of the enclosure increases faster, due to the acceleration of heat transfer by the natural convection. Also, the slope of the diagram in its initial part is the same for different Rayleigh numbers, because the Rayleigh number does not affect the conduction heat transfer.

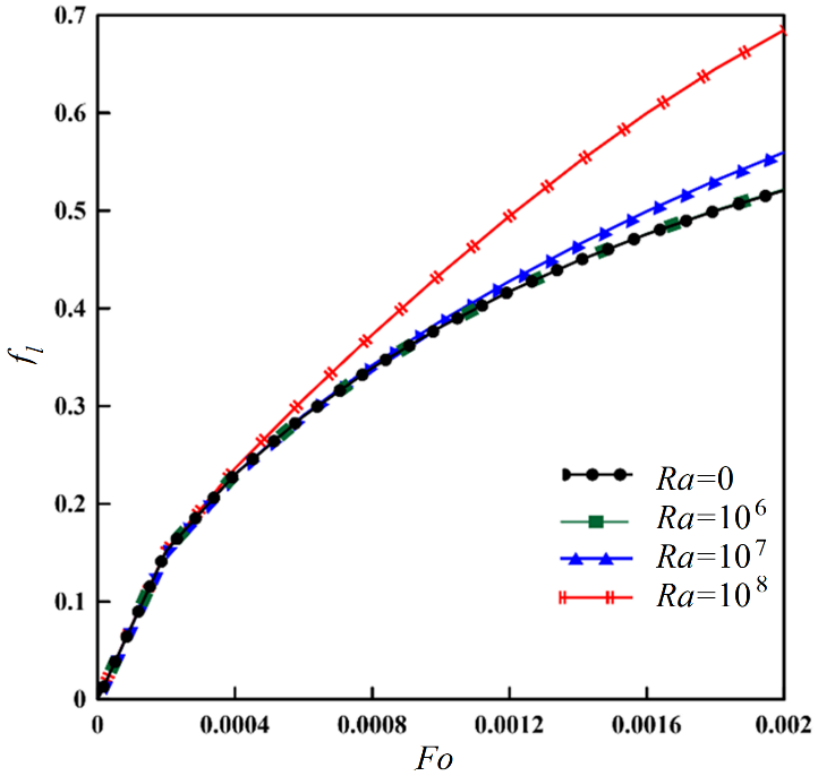

Fig. 8. Variation of the liquid fraction with respect to the dimensionless time at four Rayleigh numbers.

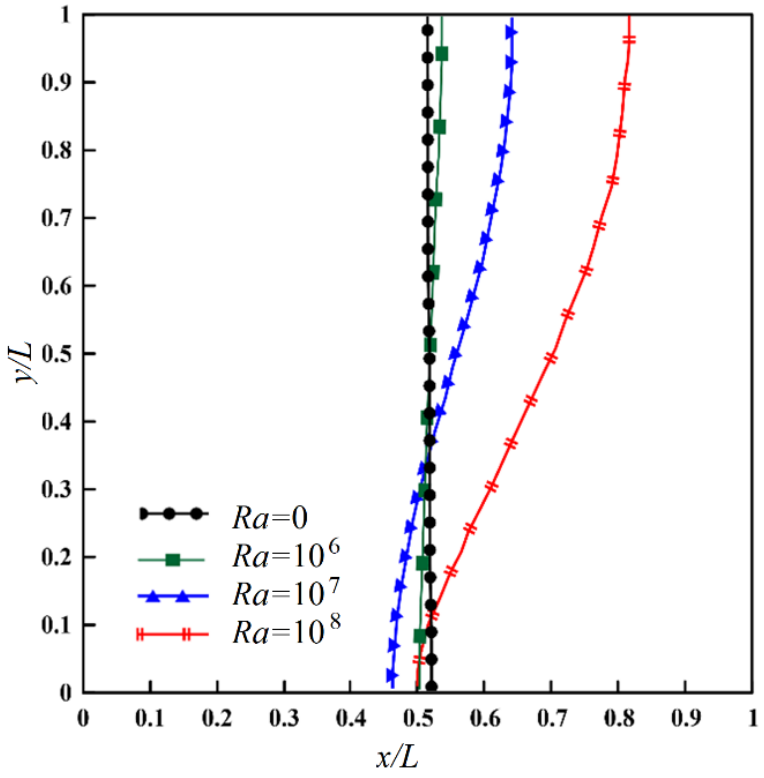

Fig. 9. Variation of the liquid fraction with respect to the dimensionless time in Fo=0.002 for different Rayleigh numbers.

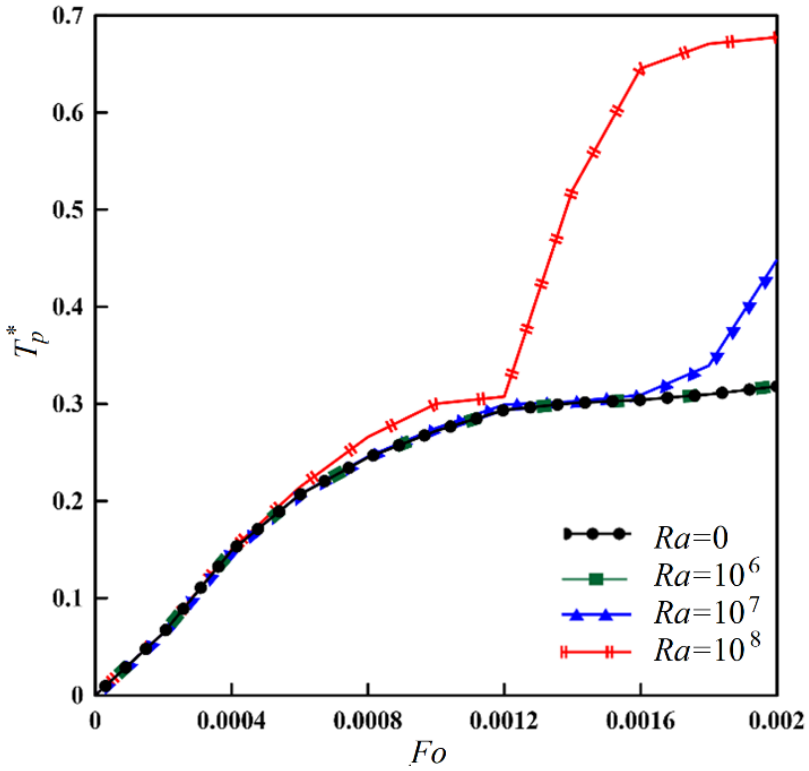

Fig. 10. Temperature of the node in the middle of the enclosure with time for different Rayleigh numbers.

Table. 4. The detailed numerical values for all parameters used in case 2 (Effect of porosity ratio).

δ	Pr	Da	Ra	Ste	Sp	F_ε	η	Nu_d	T^*_{melt}	$\tau_{t,f}$
0.0135	50	10^{-4}	10^8	1	12000	0.068	1	5.9	0.3	0.501

5- 3- Effect of porosity ratio

The porosity ratio represents the share of metal in the porous medium, so that $\varepsilon = 0$ indicates that the whole space is filled with metal, and $\varepsilon = 1$ indicates that the whole space is filled with PCM (without any metal solids). Here, three porosity ratios of 0.3, 0.8, and 0.93 are tested and the other numerical parameters are listed in Table 4. Similar to the previous cases, Fig. 11 shows the temperature contours for the PCM and the porous medium at Fo=0.002 by the color spectrum and solid lines at 9 levels along with the streamlines within the liquid phase, respectively. Since the amount of porosity in this figure (ε=0.3) is reduced compared to Fig. 4 (ε=0.8), so the velocity field and consequently the natural convection within the liquid phase is weakened and the curvature of the melting front is reduced.

Fig. 12 displays the effect of the porosity ratio on the liquid fraction. As mentioned, by increasing the porosity ratio, the share of solid metal in the enclosure decreases, this solid metal acts as a fin inside the enclosure and transfers heat throughout the enclosure. As a result, as the share of solid metal decreases, heat is transferred slowly into the enclosure and the liquid fraction is reduced. Therefore, it can be concluded that there is an inverse relationship between the porosity ratio and the liquid fraction. Fig. 13 shows the position of the melting front at Fo=0.002 for different porosity ratios. According to the diagram, as the porosity ratio decreases, the melting front progresses further, but its curvature decreases, and vice versa. The reason for this is that by reducing the porosity ratio, the heat transfer tends to pure conduction, and therefore the curvature of the melting front decreases. However, due to the large thermal conductivity of the solid matrix and also the reduction of PCM volume, the position of the melting front in small porosities is ahead of larger porosities. Also, in high porosity ratios, the predominant mechanism of heat transfer is convection, which increases the curvature of the melting front.

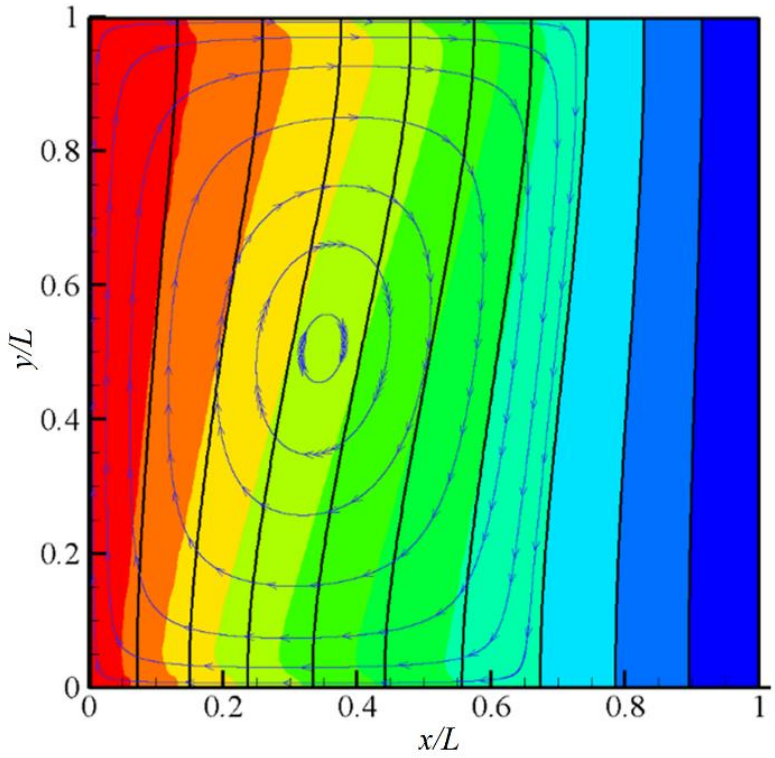

Fig. 11. Temperature contour for the PCM and porous medium at Fo=0.002 specified by the color spectrum and solid lines, respectively, in 9 levels along with streamlines in the liquid phase (ε=0.3).

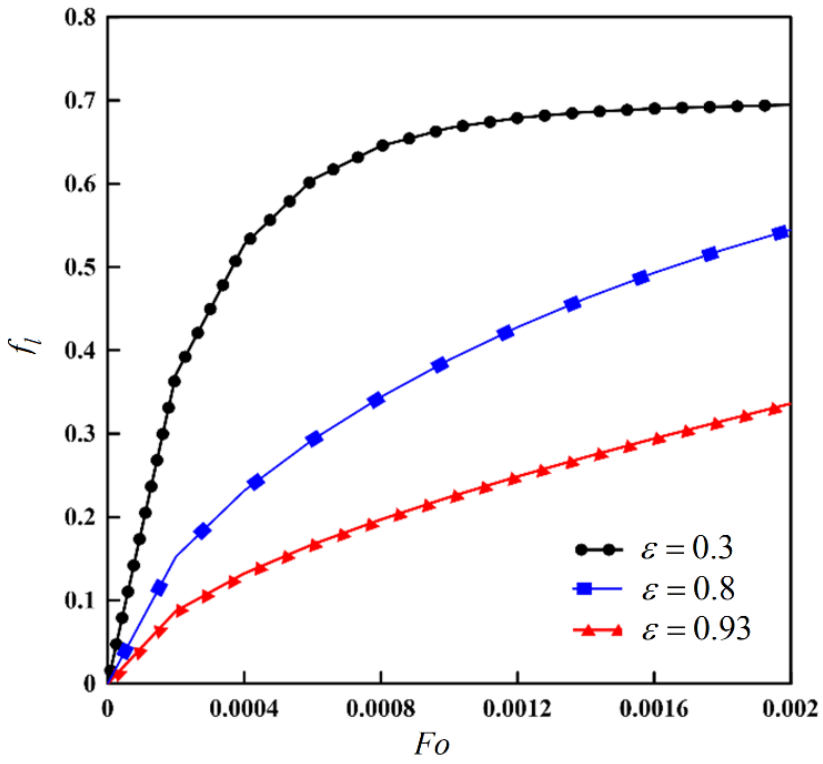

Fig. 12. Variation of the liquid fraction with respect to the time for three porosity ratios.

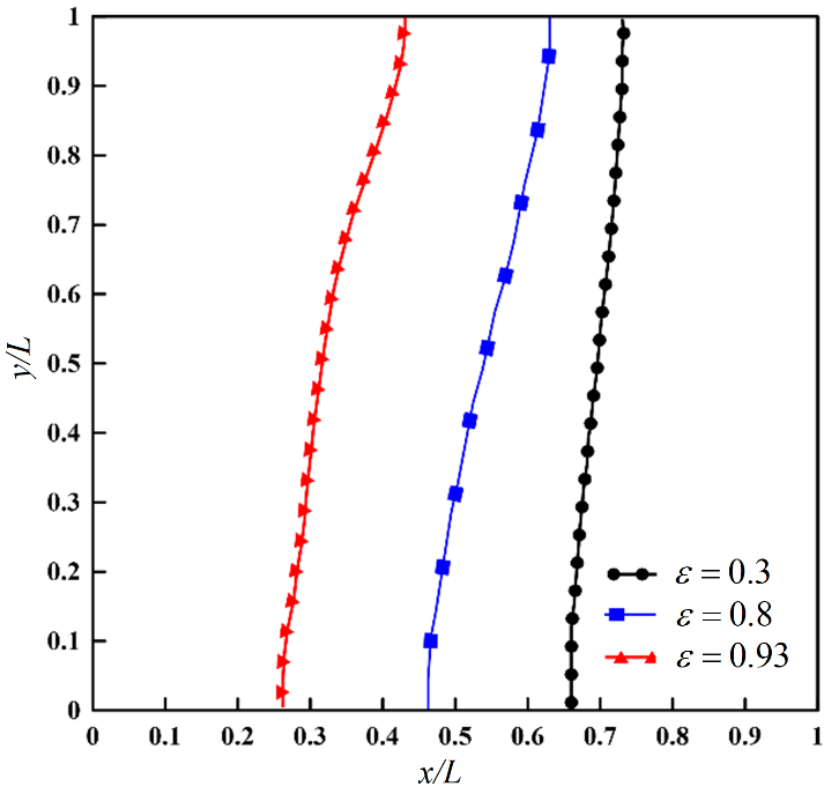

Fig.13. Position of the melting front at Fo=0.002 for three porosity ratios.

Table. 5. The detailed numerical values for all parameters used in case 3 (effects of pore diameter).

ε	Pr	Da	Ra	Ste	Sp	F_ε	η	Nu_d	T^*_{melt}	$\tau_{t,f}$
0.8	50	10^{-4}	10^8	1	12000	0.068	1	5.9	0.3	0.501

5- 4- Effect of pore diameter to enclosure length (d_p/L)

In this section, for the sake of simplicity, the term ratio of diameter to length refers to the ratio of pore diameter to enclosure length. To evaluate the effects of pore diameter, three ratios of diameter to length of δ=0.007, δ=0.0135, and δ=0.03 are selected (case 4) and other numerical values are reported in Table 5. Given the constant Sparrow and Nusselt numbers, and owing to Eq. (11), by decreasing the ratio of diameter to length δ, the ratio of effective thermal conductivity to the thermal conductivity of the PCM, k_e/k_{fl} is increased. This increases the rate of heat transfer by the conduction and increases the liquid fraction by decreasing the δ (see Fig. 14).

Increasing the conduction mechanism by decreasing the ratio of diameter to length is also shown in Fig. 15.

According to this figure, it is observed that by decreasing this ratio, along with increasing the liquid fraction, the melting front becomes flattered and its curvature decreases, which means that the natural convection decreases.

5- 5- Effect of Sparrow number

In order to compare the local convection with the conduction heat transfer, the definition of Sparrow number is used. According to Eq. (11), the Sparrow number is obtained by multiplying the Nusselt number, Nu_d by the ratio of PCM conductivity to equivalent thermal conductivity, k_{fl}/k_e times the ratio of enclosure length to the pore diameter, L/d_p. In this section, only the Sparrow number is changed and other dimensionless numbers are similar to the base condition. Therefore, by changing the Sparrow number, only the ratio of PCM conductivity to the effective thermal conductivity will be changed. Accordingly, three Sparrow numbers equal to 750, 12000, and 150000 are selected. Table 6 shows the numerical parameters used in case 4.

The thermal conductivity of the porous medium to the PCM, k_s/k_{fl} is obtained in these three Sparrow numbers according to Table 7.

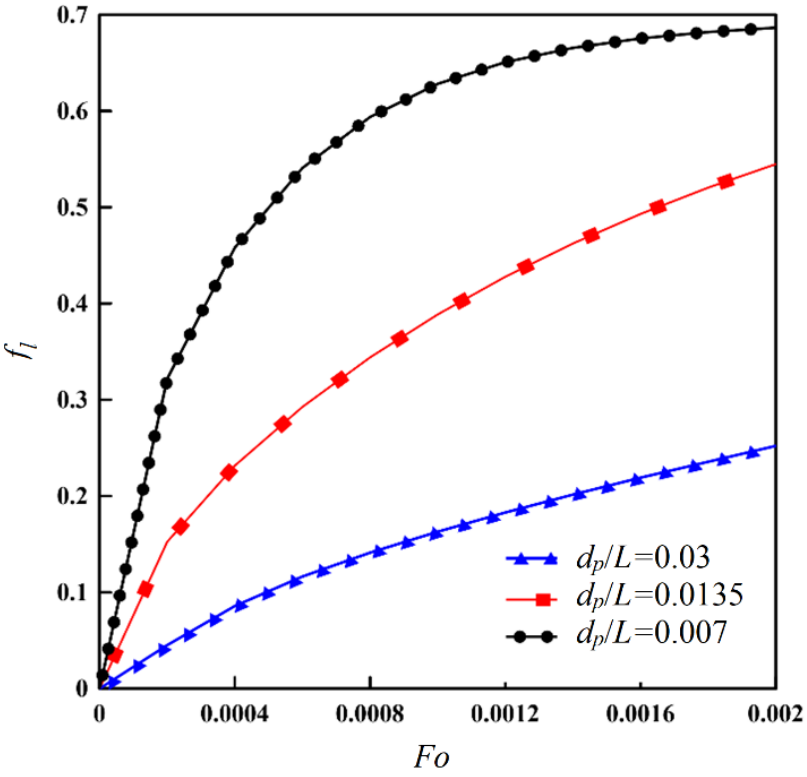

Fig. 14. Variation of liquid fraction for the different ratios of diameter to length.

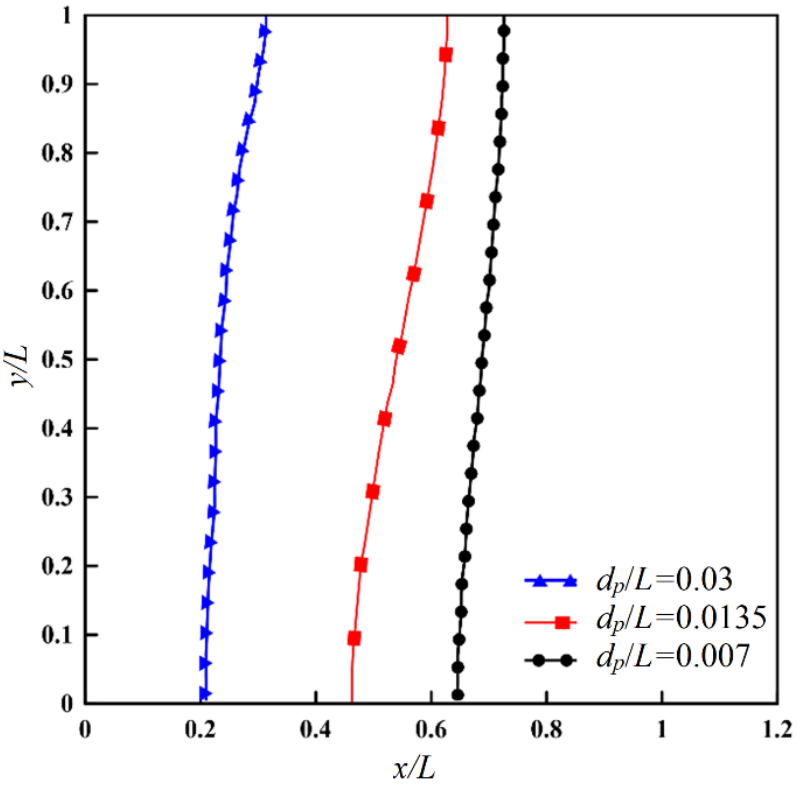

Fig. 15. Position of Melting front for different diameter to length ratios at Fo=0.002.

Table. 6. The detailed numerical values for all parameters used in case 4 (effects of Sparrow number).

ε	δ	Pr	Da	Ra	Ste	F_ε	η	Nu_d	T^*_{melt}	$\tau_{t,f}$
0.8	0.0135	50	10^{-4}	10^8	1	0.068	1	5.9	0.3	0.501

Table. 7. Ratio of PCM conductivity to the effective thermal conductivity of the solid matrix corresponding to the Sparrow number.

Sp	750	12000	150000
k_s/k_f	15982	995	76

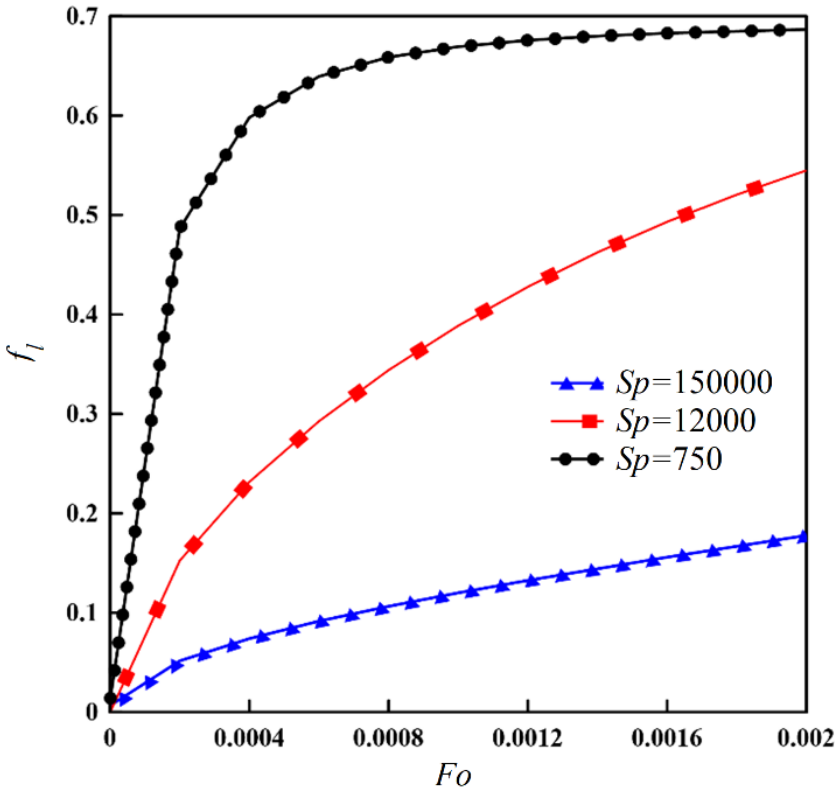

Fig. 16. The liquid fraction variation with time for different Sparrow numbers.

Fig. 16 illustrates the liquid fraction variation with time for different Sparrow numbers. By increasing the Sparrow number, the thermal conductivity of the solid matrix decreases. Hence, the conduction inside the enclosure is weakened and consequently less PCM melts compared to the small Sparrow numbers. Also in Fig. 17 the position of the melting front at Fo=0.002 is shown for different Sparrow numbers. It is quite clear that by reducing the Sparrow number, the melting front advances further, and more PCM melts. Also, as the Sparrow number decreases, the curvature of the melting front decreases. The reason for this is that by reducing the Sparrow number and increasing the thermal conductivity of the porous medium, the conduction mechanism is strengthened against the natural convection and thus the effects of natural convection that lead to the curvature of the front are reduced.

At the end of this paper, the effect of natural convection on the melting rate of the PCM is investigated. To do this, the results of the liquid fraction are compared in two cases with and without natural convection and the deviation of liquid fraction between these two conditions, D is defined as:

$$D = \frac{f_l^{NC} - f_l^{PC}}{f_l^{PC}} \times 100 \tag{35}$$

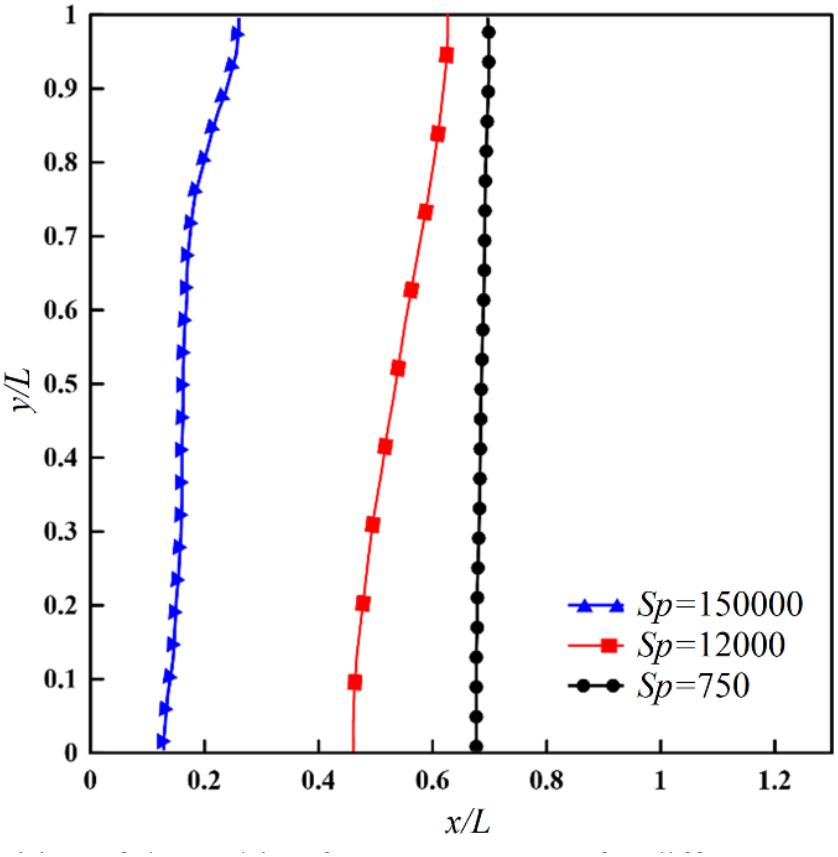

Fig. 17. The position of the melting front at Fo=0.002 for different Sparrow numbers.

where superscripts of NC and PC refer to the natural convection and pure conduction, respectively. First, the deviation of the liquid fraction, D for different Sparrow numbers and different Rayleigh numbers at Fo=0.003 and Fo=0.006 are presented in Fig. 18. As can be seen, the deviation of the liquid fraction up to $Ra=10^6$ and Fo<0.006 is almost zero. But for $Ra=10^8$ a significant deviation for the liquid fraction appears.

The reason for this is that by increasing the Rayleigh number, the natural convection increases, and the melting rate of the PCM is enhanced compared to pure conduction. Also, by increasing the Sparrow number and reducing the thermal conductivity of the solid matrix, the role of the conduction decreases, and therefore natural convection plays a more important role which causes a deviation of liquid fraction from the pure conduction. Next, the deviation of liquid fraction for different Darcy and Sparrow numbers in two dimensionless times is investigated. According to Fig. 19, it is observed that by increasing the Darcy number, the deviation increases because with increasing the Darcy number, the permeability increases, and the heat transfer is enhanced by the natural convection due to the strengthening of the velocity field.

Also, over time, the deviation increases due to the increase in the melting rate. The important point of the diagram in Fig. 19 is that the deviation of the liquid fraction has a maximum value for the $Da=10^{-2}$. The reason for ascending at the beginning of the diagram is that by increasing the Sparrow number and thus decreasing the thermal conductivity of the solid matrix, the pure conduction is weakened, and therefore the deviation increases by increasing the Sparrow number. With a further increase in the Sparrow number and further decrease of thermal conductivity of the solid matrix, the heat transfer to the solid PCM becomes weaker, resulting in a reduction of malting rate and consequently decrease of deviation of the liquid fraction. In other words, for the Sparrow numbers larger than a certain value, the thermal conductivity of the solid matrix controls the rate of melting, and for the Sparrow numbers smaller than that, the natural convection controls the rate of melting. For example, according to Fig. 19, for $Da= 10^{-2}$ and Fo= 0.003, this critical value for Sparrow number is 37500.

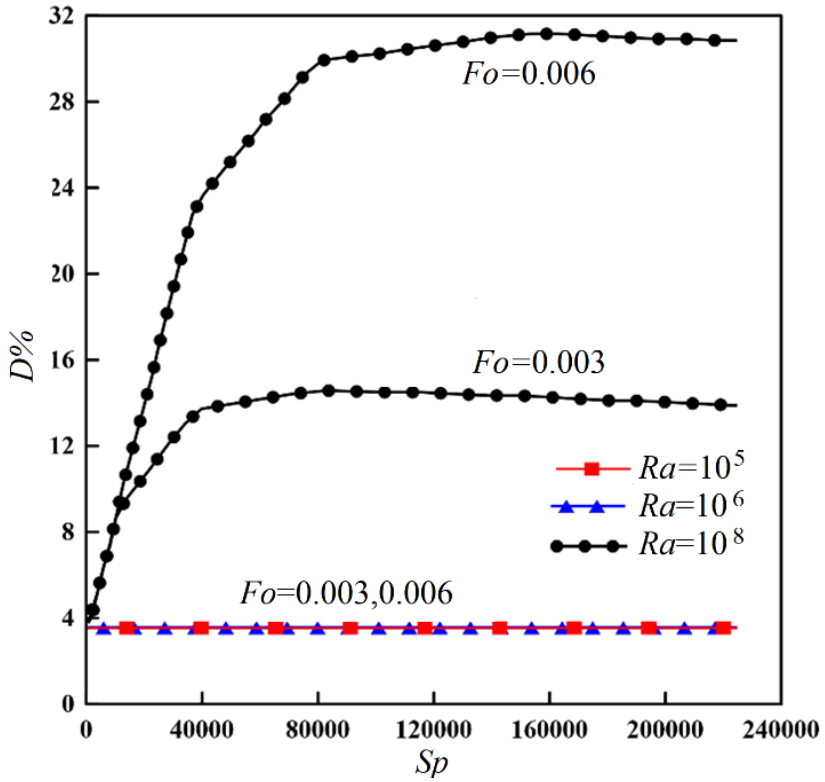

Fig. 18. Deviation of the liquid fraction compared to pure conduction under different Rayleigh numbers and different Sparrow numbers at Fo=0.003 and Fo=0.006.

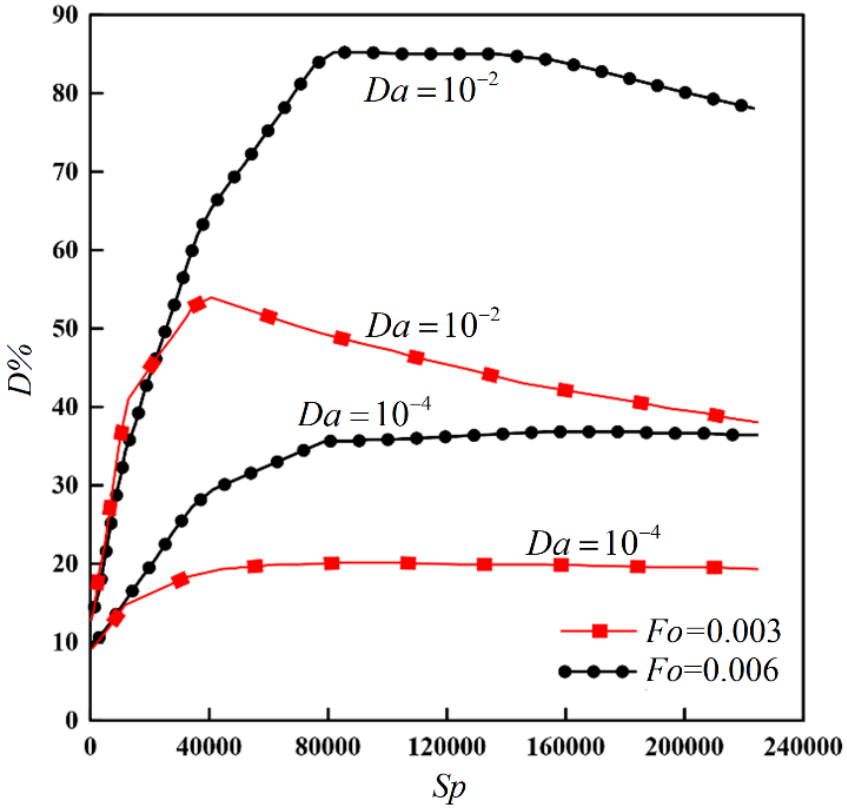

Fig. 19. Deviation of the liquid fraction compared to pure conduction under different Darcy and Sparrow numbers at Fo=0.003 and Fo=0.006.

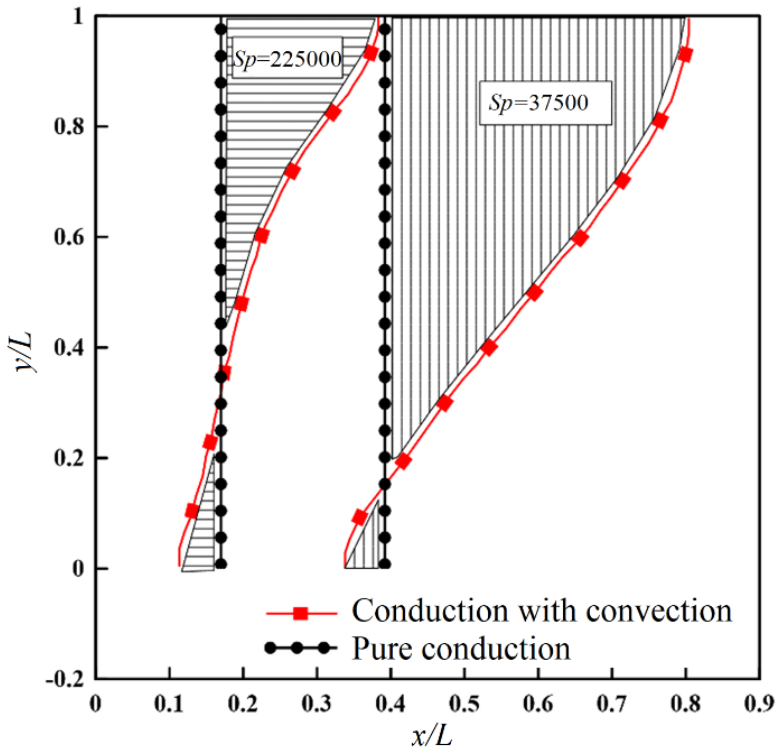

Fig. 20. Position of melting front for pure conduction and natural convection at Fo=0.003 and Da=10-2.

Fig. 20 shows a comparison between the position of the melting front in two cases of pure conduction and natural convection for Sp=37500 and Sp=225000 at Fo=0.003 and Da= 10^{-2}. In this figure, two shaded areas are seen for both Sparrow numbers. Also, the position of the melting front in the pure conduction condition is plotted in a vertical line. Due to this figure, in both conditions, the liquid fraction deviates from the net conduction. But for Sp=37500, the difference is greater. As can be seen, in this case, the difference between the area of the upper shadow and the lower shadow is large which means that the effects of natural convection are high. However, for Sp=225000, this difference has decreased, and as a result, the net liquid fraction has approached the net conduction conditions.

6- Conclusions

In this study, the process of PCM melting in a porous medium under the local thermal non-equilibrium condition was investigated using the lattice Boltzmann method. For this purpose, in addition to solving the velocity equations, two energy equations were solved, one for the PCM and the other for the porous medium. The effects of effective parameters such as Rayleigh number, Sparrow number, porosity ratio, and pore diameter to enclosure length were examined. Also, the conditions where the role of the natural convection in the melting process is weakened were studied. The results showed that:

1. It is seen that for small Rayleigh numbers (Ra<10^6) the rate of advance of the melting front at the top of the enclosure is almost equal to the rate of lag at the bottom of the enclosure, and therefore the amount of liquid fraction in these conditions does not differ from the pure conduction. Also, it is shown that with increasing the Rayleigh number, the mushy zone becomes smaller and the temperature of the point located in the center of the enclosure increases faster.
2. As the porosity decreases, the progress of the melting front increases but its curvature decreases. This is due to the weakening of the natural convection as well as the reduction of the volume of the phase change material.
3. It is seen that by increasing the pore diameter, the natural convection increases which cause the melting front to bend, but the liquid fraction decreases.
4. In the small Darcy numbers, the deviation of liquid fraction from the pure conduction is always ascending function of the Sparrow number, but for the large Darcy numbers, this deviation has a maximum value.

Finally, the following points can be suggested for future studies. Here, a constant convective heat transfer coefficient was used to apply the local thermal non-equilibrium condition. Existing correlations can be used to approximate the local heat transfer coefficient in terms of Prandtl and Reynolds numbers. Also, the study of time-dependent boundary conditions instead of the constant temperature can show the effects of changes in the amplitude and frequency of the boundary temperature on strengthening or weakening the local thermal non-equilibrium condition.

Nomenclature

$_{cp}$	Specific heat at constant pressure
c_s	Lattice sound speed
$D\%$	Deviation percentage
Da	Darcy number, $Da=K/L^2$
d_p	Pore diameter
$\boldsymbol{e_i}$	Discrete lattice velocity
En	Enthalpy
f_l	Liquid fraction of the PCM
f_i	Density distribution function
$\boldsymbol{F}$	Body force per unit mass
F_i	Discrete body force
Fo	Fourier number, $Fo=\alpha_f t/L^2$
F_ε	Forchheimer coefficient
$\boldsymbol{g}$	Acceleration due to gravity
g_i	Temperature distribution function
h_v	Volumetric heat transfer coefficient
J	Equivalent kinematic viscosity to the kinematic viscosity of the PCM
k	Thermal conductivity
K	Permeability
L_a	Latent heat of melting
L	Characteristic length
m	Mass
N	Arbitrary distribution function
Nu_d	Interfacial Nusselt number based on the pore diameter, $Nu_d = h_v d_p^2 / k_{fl}$
p	Pressure
Pr	Prandtl number, $Pr = \upsilon_f / \alpha_f$
Ra	Rayleigh number, $Ra = \dfrac{g\beta\Delta T L^3}{\upsilon_{fl}\alpha_{fl}}$
Sp	Sparrow number, $Sp = \dfrac{hL^3}{k_e d_p}$
Sr_i	Source term due to local non-equilibrium condition
Su_i	Discrete source term to correct the energy equation
Ste	Stefan number, $Ste = \dfrac{c_{p,f}\Delta T}{L_a}$
t	Time
T	Temperature
T_p	Mid-point temperature
$\boldsymbol{u}$	Velocity
$\boldsymbol{v}$	Temporal velocity
V	Volume
V_p	Volume of the empty space
$_{wi}$	Weight factor
x,y,z	Cartesian coordinates

Greek symbols

α	Thermal diffusivity
β	Coefficient of thermal expansion
γ	Free parameter in the equilibrium distribution function
δ	Pore diameter to the characteristic length
δt	Time step
Δx	Lattice space
ε	Porosity
η	Porous heat capacity to PCM heat capacity
ν	Kinematic viscosity
ρ	Density
τ_f , τ_t	Dimensionless relaxation time
Ω	Collision parameter

Subscripts

b	Boundary
$begin$	Beginning of the melting
e	Effective or equal
end	End of the melting
f	fluid
fl	Liquid phase of the PCM
i	The ith direction in a lattice
L	Left wall
n	Neighbor
R	Right wall
ref	Reference value
s	Solid matrix

Superscript

eq	Equilibrium
neq	Non- equilibrium
$*$	Dimensionless value

References

[1] F. Agyenim, N. Hewitt, P. Eames, M. Smyth, A review of materials, heat transfer and phase change problem formulation for latent heat thermal energy storage systems (LHTESS), Renewable and sustainable energy reviews, 14(2) (2010) 615-628.

[2] M. Gaeini, S. Shaik, C. Rindt, Characterization of potassium carbonate salt hydrate for thermochemical energy storage in buildings, Energy and Buildings, 196 (2019) 178-193.

[3] M. Nakhchi, J. Esfahani, Improving the melting performance of PCM thermal energy storage with novel stepped fins, Journal of Energy Storage, 30 (2020) 101424.

[4] C. Nie, S. Deng, J. Liu, Effects of fins arrangement and parameters on the consecutive melting and solidification of PCM in a latent heat storage unit, JOURNAL OF ENERGY STORAGE, 29 (2020).

[5] S. Rostami, M. Afrand, A. Shahsavar, M. Sheikholeslami, R. Kalbasi, S. Aghakhani, M.S. Shadloo, H.F. Oztop, A review of melting and freezing processes of PCM/nano-PCM and their application in energy storage, Energy, 211 (2020) 118698.

[6] L. Yang, J.-n. Huang, F. Zhou, Thermophysical properties and applications of nano-enhanced PCMs: An update review, Energy Conversion and Management, 214 (2020) 112876.

[7] A. Ghahremannezhad, H. Xu, M.R. Salimpour, P. Wang, K. Vafai, Thermal performance analysis of phase change materials (PCMs) embedded in gradient porous metal foams, Applied Thermal Engineering, 179 (2020) 115731.

[8] R. Mabrouk, H. Dhahri, H. Naji, S. Hammouda, Z. Younsi, Lattice Boltzmann simulation of forced convection melting of a composite phase change material with heat dissipation through an open-ended channel, International Journal of Heat and Mass Transfer, 153 (2020) 119606.

[9] Y. Tao, Y. You, Y. He, Lattice Boltzmann simulation on phase change heat transfer in metal foams/paraffin composite phase change material, Applied Thermal Engineering, 93 (2016) 476-485.

[10] M. Jourabian, A.A.R. Darzi, D. Toghraie, O. ali Akbari, Melting process in porous media around two hot cylinders: Numerical study using the lattice Boltzmann method, Physica A: Statistical Mechanics and its Applications, 509 (2018) 316-335.

[11] D. Gao, Z. Chen, D. Zhang, L. Chen, Lattice Boltzmann modeling of melting of phase change materials in porous media with conducting fins, Applied Thermal Engineering, 118 (2017) 315-327.

[12] D. Gao, Z. Chen, Lattice Boltzmann simulation of natural convection dominated melting in a rectangular cavity filled with porous media, International Journal of Thermal Sciences, 50(4) (2011) 493-501.

[13] D. Gao, F.-B. Tian, Z. Chen, D. Zhang, An improved lattice Boltzmann method for solid-liquid phase change in porous media under local thermal non-equilibrium conditions, International Journal of Heat and Mass Transfer, 110 (2017) 58-62.

[14] W. Minkowycz, A. Haji-Sheikh, K. Vafai, On departure from local thermal equilibrium in porous media due to a rapidly changing heat source: the Sparrow number, International journal of heat and mass transfer, 42(18) (1999) 3373-3385.

[15] D. Gao, Z. Chen, L. Chen, A thermal lattice Boltzmann model for natural convection in porous media under local thermal non-equilibrium conditions, International Journal of Heat and Mass Transfer, 70 (2014) 979-989.

[16] C. Wang, M. Mobedi, F. Kuwahara, Analysis of local thermal non-equilibrium condition for unsteady heat transfer in porous media with closed cells: Sparrow number, International Journal of Mechanical Sciences, 157 (2019) 13-24.

[17] M. Esapour, A. Hamzehnezhad, A.A.R. Darzi, M. Jourabian, Melting and solidification of PCM embedded in porous metal foam in horizontal multi-tube heat storage system, Energy conversion and management, 171 (2018) 398-410.

[18] Q. Liu, X.-B. Feng, X.-L. Wang, Multiple-relaxation-time lattice Boltzmann model for convection heat transfer in porous media under local thermal non-equilibrium condition, Physica A: Statistical Mechanics and its Applications, 545 (2020) 123794.

[19] A. Amiri, K. Vafai, Analysis of dispersion effects and non-thermal equilibrium, non-Darcian, variable porosity incompressible flow through porous media, International journal of heat and mass transfer, 37(6) (1994) 939-954.

[20] G. Zhao-Li, Z. Chu-Guang, S. Bao-Chang, Non-equilibrium extrapolation method for velocity and pressure boundary conditions in the lattice Boltzmann method, Chinese Physics, 11(4) (2002) 366.

[21] X. He, S. Chen, G.D. Doolen, A novel thermal model for the lattice Boltzmann method in incompressible limit, Journal of computational physics, 146(1) (1998) 282-300.

HOW TO CITE THIS ARTICLE

M. Taghilou , S. A. Safavi , A Parametric Investigation of Melting Process within a Porous Medium under Local Thermal Non-Equilibrium Condition Using Lattice Boltzmann Method, AUT J. Mech Eng., 6 (3) (2022) 467-488.

DOI: 110.22060/ajme.2022.20383.5997